

Optical selection rules of the magnetic excitation in the $S = \frac{1}{2}$ one-dimensional Ising-like antiferromagnet $\text{BaCo}_2\text{V}_2\text{O}_8$

Shojiro Kimura *Institute for Materials Research, Tohoku University, Katahira 2-1-1, Sendai 980-8577, Japan*

Hiroaki Onishi

Advanced Science Research Center, Japan Atomic Energy Agency, Tokai, Ibaraki 319-1195, Japan

Akira Okutani

Research Center for Development of Far-Infrared Region, University of Fukui, Fukui, Fukui 910-8507, Japan

Mitsuru Akaki

Molecular Photoscience Research Center, Kobe University, Kobe 657-8051, Japan

Yasuo Narumi and Masayuki Hagiwara

Center for Advanced High Magnetic Field Science, Graduate School of Science, Osaka University, Toyonaka Osaka 560-0043, Japan


Kouichi Okunishi

Department of Physics, Niigata University, Niigata 950-2181, Japan

Koichi Kindo

*Institute for Solid State Physics, University of Tokyo, Kashiwa 277-8531, Japan*Zhangzhen He *State Key Laboratory of Structural Chemistry, Fujian Institute of Research on the Structure of Matter, Chinese Academy of Sciences, Fuzhou 350002, People's Republic of China*

Tomoyasu Taniyama

*Department of Physics, Nagoya University, Nagoya, 464-8602, Japan*Mitsuru Itoh *National Institute of Advanced Industrial Science and Technology, Tsukuba, Ibaraki 305-8568, Japan*

(Received 13 July 2021; revised 13 October 2021; accepted 4 January 2022; published 18 January 2022)

In this study, we clarify the selection rules of optical transitions from the ground state to the magnetic excited states in the quasi-one-dimensional quantum Ising-like antiferromagnet $\text{BaCo}_2\text{V}_2\text{O}_8$ with spin $S = \frac{1}{2}$ using the high-field electron spin resonance measurement with illuminating polarized electromagnetic waves. We demonstrate that the unconventional magnetic excitation via the pair creation of quasiparticles at wave numbers $q_z = \pi/2$ and π in the field-induced quantum critical state can couple with both oscillating magnetic and electric fields. Our density matrix renormalization group calculations indicate that the observed selection rules can be explained by two- and four-fold periodical spin interactions, originating from the screw chain structure in $\text{BaCo}_2\text{V}_2\text{O}_8$, in addition to the magnetoelectric coupling between spins and electric dipoles.

DOI: [10.1103/PhysRevB.105.014417](https://doi.org/10.1103/PhysRevB.105.014417)

I. INTRODUCTION

Low-lying magnetic excitation in a one-dimensional (1D) antiferromagnetic quantum spin (S) chain has garnered the interest of researchers for a long time since Bethe proposed a method to obtain exact eigenvalues and eigenstates for the system with $S = \frac{1}{2}$ in 1931 [1]. For the isotropic Heisenberg chain with $S = \frac{1}{2}$, the quantum fluctuation inherent in

the system destroys the long-range magnetic order, thereby leading to a quantum critical ground state. The magnetic excitation from this considerably fluctuating ground state exhibits marked contrast to a classical spin wave. The lowest magnetic excitation in the quantum system at a zero magnetic field forms an unconventional energy continuum of spin triplet states with 2π periodicity, which consist of a pair excitation of quasiparticles called spinon, i.e., a mobile quantum

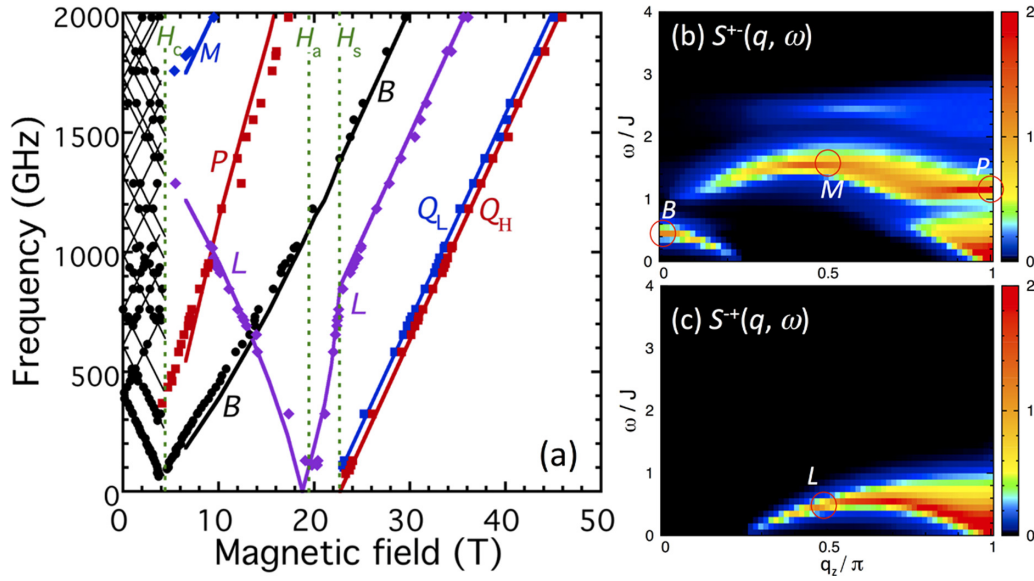


FIG. 1. (a) ESR resonance points observed in $\text{BaCo}_2\text{V}_2\text{O}_8$ for $H \parallel c$ [17]. The bold solid curves above H_c are the magnetic excitation energies at $q = 0, \pi/2$, and π , obtained from our previous calculations [17]. The thin solid lines below H_c are guides for the eyes. The magnetic structure factors (b) $S^+(q, \omega)$ and (c) $S^-(q, \omega)$ obtained from the DMRG calculation for the $S = \frac{1}{2}$ quantum Ising-like chain with $\epsilon = 0.46$ in the longitudinal magnetic field, where the total magnetization reaches to 1/4 of the saturation. The ESR signals B and L in the quantum critical phase emerge from the psinon-antipsinon pair excitation at $q_z = 0$ and the psinon-psinon pair excitation at $q_z = \pi/2$, respectively. The M and P originate from the two-string excitations at $q_z = \pi/2$ and $q_z = \pi$, respectively. For the calculation of the $S^+(q, \omega)$ and $S^-(q, \omega)$, J_π and $J_{\pi/2}$ are not included.

domain wall carrying fractional quantum number $S = \frac{1}{2}$ [2–7]. In the application of magnetic fields, the situation becomes more intricate. The quantum critical ground state with a finite magnetization in magnetic fields up to the saturation field H_s is partially filled by magnons, which correspond to overturned spins from the fully polarized spin state [8]. Then, the lowest-energy excitation is governed by scattering states of the quasiparticles psinons and antipsinons, which are holes and particles created into the ground state [9,10] (see Appendix A for detail). As a result, the transverse and longitudinal excitation owing to the pair creation of these quasiparticles are gapless at the incommensurate soft wave vectors $q_z = \pi, \pm 2\pi m$ and $q_z = 0, \pi \pm 2\pi m$, respectively, where m represents the magnetization per spin [5,9–12]. Furthermore, a recent theory has indicated that, in addition to the scattering states, the string states, which are characterized by complex rapidities in Bethe-ansatz calculations [13,14], and therefore change asymptotically to multi-magnon bound states upon increasing the field to H_s , significantly contribute to the dynamical correlation function in the magnetic field [15,16].

The experimental verification of the nontrivial behaviors of the $S = \frac{1}{2}$ quantum spin chain in magnetic fields is a demanding task. A suitable compound for the investigations is the quasi-1D antiferromagnet $\text{BaCo}_2\text{V}_2\text{O}_8$ with the intrachain exchange interaction described by the following Ising-like XXZ Hamiltonian with $\epsilon \simeq 0.5$ and $J \simeq 65$ K [17].

$$\mathcal{H} = J \sum_j \{S_j^z S_{j+1}^z + \epsilon (S_j^x S_{j+1}^x + S_j^y S_{j+1}^y)\}. \quad (1)$$

Different from the Heisenberg system, the ground state of the Ising-like chain maintains Néel order at zero magnetic field. However, in applied magnetic fields along the longitudinal z direction, a quantum phase transition from the Néel ordered state to the quantum critical state, which belongs to a universality class called Tomonaga-Luttinger liquid (TLL), as well as that of the Heisenberg system, occurs [18]. In fact, the spin density wave (SDW) order, for which the longitudinal incommensurate correlation characteristic of the TLL develops to the long-range order under the influence of inevitable interchange interactions, has been found in $\text{BaCo}_2\text{V}_2\text{O}_8$ above the transition field $H_c \simeq 3.9$ T [19–22]. The energy minimum of the longitudinal excitation at an incommensurate wave vector was also observed [23]. Overall behaviors of the magnetic excitation in the quantum critical state above H_c were elucidated via high-field electron spin resonance (ESR) measurements of $\text{BaCo}_2\text{V}_2\text{O}_8$ up to 50 T [17]. As shown in Fig. 1(a), six kinds of the resonance modes B, L, M, P, Q_L , and Q_H were observed above H_c . Detailed comparison with the numerical calculation indicated that the B, L , and M and P emerge from the magnetic excitations at $q_z = 0, \pi/2$, and π , respectively, as presented in Figs. 1(b) and 1(c). The softening of L at $H_a \simeq 19$ T, where the m reaches a half of its saturation value, is a manifestation of the TLL nature. The appearance of the $Q_{L,H}$ above the saturation field $H_s \simeq 22$ T indicates the reopening of the excitation gap at $q_z = \pi$. From the recent terahertz spectroscopy measurements of $\text{BaCo}_2\text{V}_2\text{O}_8$ and its sister compound $\text{SrCo}_2\text{V}_2\text{O}_8$, it was identified that the B, L , and P originate from the psinon-antipsinon pair, the psinon-psinon pair, and the two-string excitations, respectively [24,25]. The excitation spectra in energy-momentum space, observed by the subsequent

neutron scattering measurements of $\text{SrCo}_2\text{V}_2\text{O}_8$ in the quantum critical state, was successfully explained by the Bethe-anzats calculations [26]. However, there remains an unresolved issue that the optical transitions to excited states at finite wave vectors, such as the L , M , P , and $Q_{L,H}$, are forbidden by the momentum preservation law. Although the origin of the observations of these forbidden modes certainly originates from the peculiar four-fold screw Co-O chain structure in the compounds, the detailed mechanism of the observations remains unclear to date. In this study, we clarify the selection rules of the excitation modes, using the high-field ESR measurement illuminating polarized electromagnetic waves to the single crystal of $\text{BaCo}_2\text{V}_2\text{O}_8$. It turns out that the selection rule differs from the excitation mode to the mode. Surprisingly, the magnetic excitation in the quantum critical state couples with both oscillating magnetic and electric fields. Our theoretical calculations clarify that the mixing of quantum states to the ground state by two- and four-fold spin interactions originating from the screw chain structure and the spin-dependent electric dipole are the origins for the observations of the magnetic excitation at $q_z = \pi/2$ and π .

II. EXPERIMENT

We measured the polarization dependence of the ESR spectra in $\text{BaCo}_2\text{V}_2\text{O}_8$ in magnetic fields applied along the c axis, which is the easy z axis of this compound. In the measurements of the Voigt configuration, where the electromagnetic wave propagates perpendicularly to the c axis, a wire grid polarizer for linearly polarizing the electromagnetic wave is put in front of the sample. For this measurement, a single crystal, grown by a spontaneous nucleation method [27,28], was used. The oscillating magnetic h and electric e fields are applied along the $[001]$ or $[1\bar{1}0]$ by illuminating linearly polarized electromagnetic waves to the (110) plane. We also measured the ESR spectrum in the Faraday configuration with the light propagation direction parallel to the c axis by illuminating the unpolarized electromagnetic waves. For this measurement, a single crystal, grown by a floating zone method [29], was used. The measurements at electromagnetic wave frequencies 730.5 GHz and 1839 GHz were performed in pulsed magnetic fields at 1.3 K, and those at 490 GHz were carried out by utilizing a superconducting magnet at 1.5 K. From the measurements at these three frequencies, we can clarify the selection rule of all the ESR modes, namely the spinon excitation and the B , L , M , P , Q_L , and Q_H modes.

III. RESULTS

Figure 2(a) presents the ESR spectra observed in the three different configurations at 730.5 GHz. The two sharp signals in the Néel ordered state below H_c come from the quantized energy levels called Zeeman ladders, which originate from the confinement of the spinon excitation by the interchain molecular fields [30–32]. The signals from the Zeeman ladders and the signal B , which originates from the antispinon-psinon excitation at $q = 0$, are shown to couple with h perpendicular to c axis as previously reported [25] because the signal intensities significantly decrease when h is applied parallel to the c axis. The observed behaviors are consistent with the

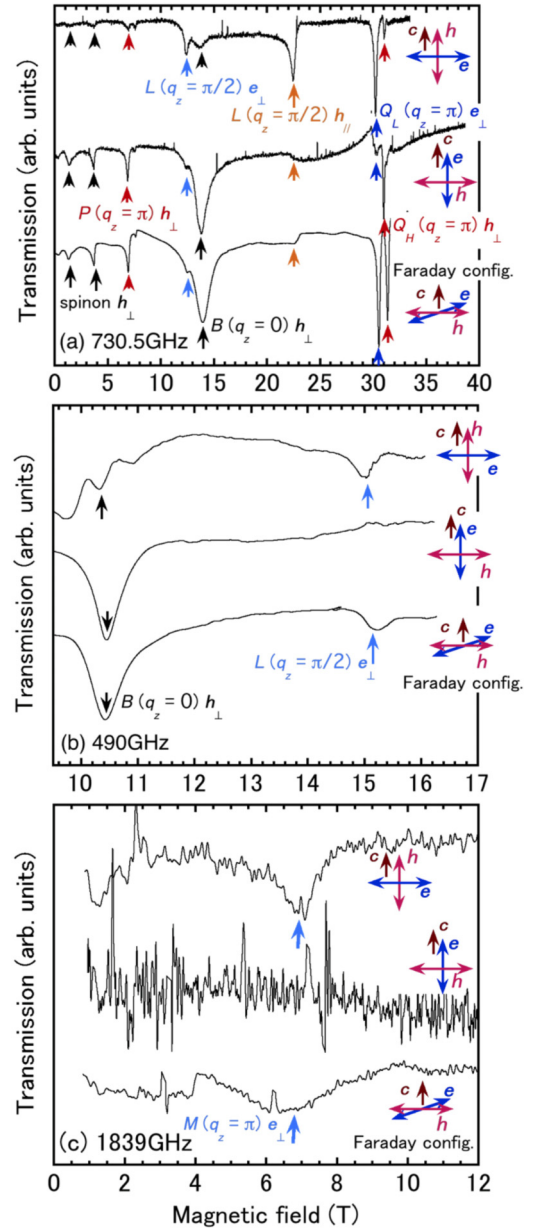
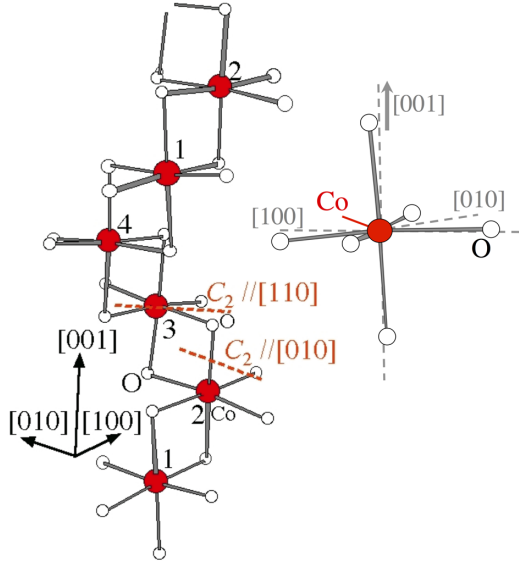


FIG. 2. ESR spectra observed in $\text{BaCo}_2\text{V}_2\text{O}_8$ for $H \parallel c$ at (a) 730.5 GHz, (b) 490 GHz, and (c) 1839 GHz. The upper and middle curves are spectra, observed by illuminating electromagnetic waves with the magnetic component polarized parallel and perpendicular to the c axis, respectively, in the Voigt configuration. The lower curves are the spectra, observed by illuminating unpolarized electromagnetic waves in the Faraday configuration.

fact that these signals come from excitations with transverse spin fluctuations at $q = 0$, which allows the usual magnetic dipole transition. In contrast, the polarization dependencies of the signals originating from the excitation to $q_z = \pi/2$ or π are significantly more complicated. The experimental results at 730.5 GHz suggest that P couples with h perpendicular to c , as well as B , while the results at 1839 GHz in Fig. 2(c) indicates M couples with e perpendicular to c . The polarization dependence of the signal L observed below H_a is not apparent from the ESR spectra at 730.5 GHz because the signal L

FIG. 3. The four-fold screw Co-O chain in BaCo₂V₂O₈.

is superimposed on the large signal of the B . However, the results at 490 GHz in Fig. 2(b) clearly indicate that the signal couples with \mathbf{e} perpendicular to c . In contrast, the L above H_a observed at 730.5 GHz around 22 T is excited by \mathbf{h} parallel to c . Hence, L is suggested to change from electroactive to magnetoactive as the static magnetic field is increased. As shown in Fig. 2(a), the signal intensities of Q_L and Q_H , which appear above H_s , are similar to each other in the Faraday configuration, whereas the results in the Voigt configuration indicate that the lower field peak Q_L is electroactive by $\mathbf{e} \perp c$, while the higher field one Q_H is magnetoactive by $\mathbf{h} \perp c$. The Q_L and Q_H are considered to come from the transitions to the excited states at $\mathbf{q} = (\pi \pi \pi)$ and $(0 0 \pi)$, respectively, as will be discussed below. The splitting between these two modes results from weak exchange interactions between Co-O chains in BaCo₂V₂O₈, which causes weak energy dependence of the magnon dispersion along the $(q_x q_x \pi)$ direction in the reciprocal lattice space. By assuming one magnon dispersion of a simple square lattice ferromagnet and $\epsilon = 0.46$, the effective interchain interaction J' is evaluated to be $J' = 2.2$ K ($J'/J = 0.034$), in agreement with the result of the inelastic neutron scattering [31].

IV. ANALYSIS AND DISCUSSION

There are two mechanisms that induce optical transitions to the magnetic excited states at wave numbers far from $q = 0$. One mechanism involves mixing between the ground and excited states by perturbative spin interactions, which yields a finite magnetic dipole transition probability, as the staggered fields proposed for the transition to the gapped spin triplet state at $q = \pi$ in the Haldane system Ni(C₂H₈N₂)₂Ni₂(ClO₄) (NENP) [33]. The other mechanism involves coupling between spins and electric dipoles, which enables to cause electric dipole transition [34–37]. Both mechanisms are governed by the crystallographic symmetry of the spin chain. As illustrated in Fig. 3, the Co-O chain in BaCo₂V₂O₈ forms a four-fold screw structure, composed of edge-shared CoO₆

octahedra [38]. The Co²⁺ ion is located on the two-fold rotation axis parallel to the [110] under rhombic ligand fields, and the nearest neighbor Co sites are connected by the two-fold rotation around the [100]. Because the apical Co-O(1) bond is inclined from the c -axis, the principal axis of the anisotropic exchange interaction between the Co²⁺ spins is inclined from the c -axis, and thereby alters the direction four-step periodically, along the chain. Previous studies demonstrated that this four-fold periodical structure significantly influence the nature of BaCo₂V₂O₈ in transverse fields [39–46]. By considering this screw chain structure, the nearest-neighbor exchange interactions in the Co-O chain can be expressed as

$$\mathcal{H} = \mathcal{H}_{\text{uni}} + \mathcal{H}_{\pi} + \mathcal{H}_{\pi/2}, \quad (2)$$

where

$$\mathcal{H}_{\text{uni}} = \sum_j J \left\{ S_j^z S_{j+1}^z + \frac{\epsilon}{2} (S_j^+ S_{j+1}^- + S_j^- S_{j+1}^+) \right\} - g\mu_B H_0 S_j^z, \quad (3)$$

$$\mathcal{H}_{\pi} = \sum_j J_{\pi} \{ \cos(\pi j) (S_j^+ S_{j+1}^+ + S_j^- S_{j+1}^-) \}, \quad (4)$$

and

$$\mathcal{H}_{\pi/2} = \sum_j J_{\pi/2} \left\{ \cos\left(\frac{\pi}{2} j\right) (S_j^x S_{j+1}^z + S_j^z S_{j+1}^x) + \sin\left(\frac{\pi}{2} j\right) (S_j^y S_{j+1}^z + S_j^z S_{j+1}^y) \right\}. \quad (5)$$

Here J_{π} and $J_{\pi/2}$ represent the exchange interactions with π and $\pi/2$ periodicity, respectively, of which detailed descriptions are given in Appendix B. The x , y , and z are defined to be parallel to the [100], [010], and [001], respectively. The \mathcal{H}_{π} and $\mathcal{H}_{\pi/2}$ mix the quantum state at $q = 0$ with those at $q_z = \pi$ and $\pi/2$, respectively, thereby resulting in finite probabilities for magnetic dipole transitions between the states. Next, we consider the electric dipole transition. From the studies on magnetoelectric effect, the electric polarization that depends on a vector spin chirality $\mathbf{P}_j = \tilde{C}(\mathbf{S}_j \times \mathbf{S}_{j+1})$ is widely recognized [35,47–51]. Here \mathbf{P}_j is the electric polarization on a pair of spins at the j and $j+1$ sites, and \tilde{C} is a second rank axial tensor, of which the form is restricted by the crystallographic symmetry between the two spin sites [51]. In the case of the Co²⁺ spin pair with a two-fold rotational symmetry, \tilde{C} is given as

$$\tilde{C} = \begin{pmatrix} 0 & C_{XY} & 0 \\ C_{YX} & 0 & C_{YZ} \\ 0 & C_{ZY} & 0 \end{pmatrix}, \quad (6)$$

where the Z and Y are parallel to the nearest-neighbor Co-Co bond and the [010], respectively, and X is perpendicular to both Y and Z . By considering the inclination of Z from the c -axis, \mathbf{P}_j are expressed in the xyz coordinates as follows:

$$\begin{aligned} P_j^x &= (A \cos(\pi j) + D) (S_j^z S_{j+1}^x - S_j^x S_{j+1}^z) \\ &+ (B - E) \sin\left(\frac{\pi}{2} j\right) (S_j^z S_{j+1}^y - S_j^y S_{j+1}^z), \end{aligned} \quad (7)$$

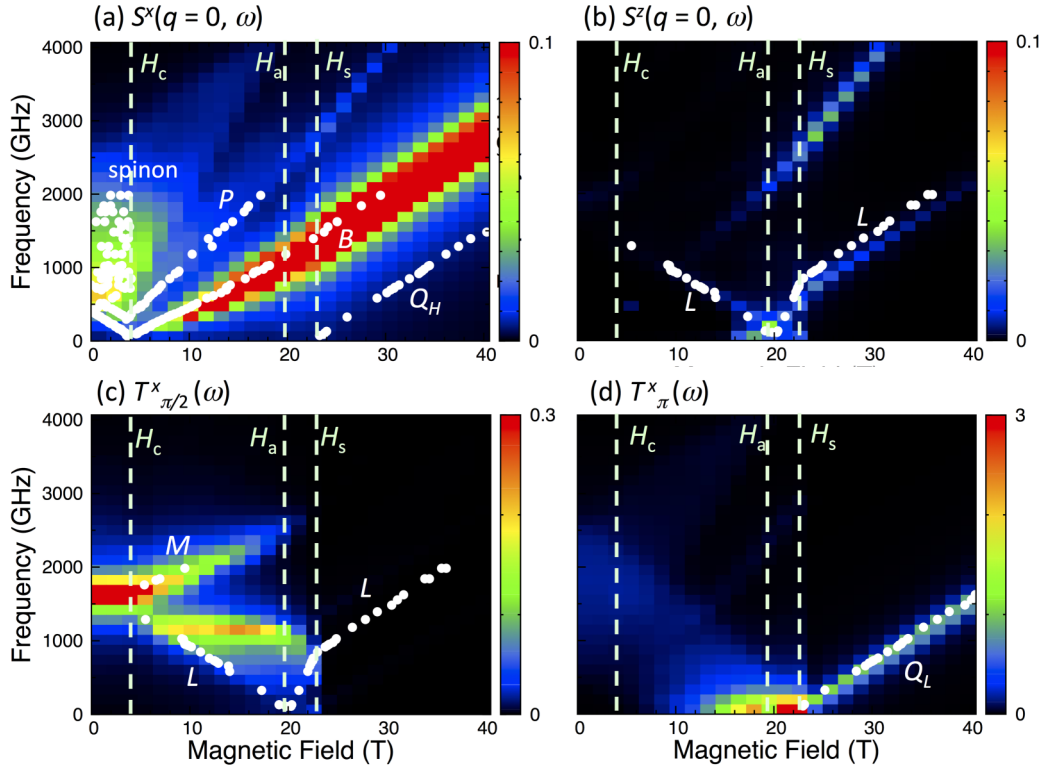


FIG. 4. Results of the DMRG calculations for (a) $S^x(q=0, \omega)$, (b) $S^z(q=0, \omega)$, (c) $T_{\pi/2}^x(\omega)$, and (d) $T_{\pi}^x(\omega)$ obtained with $J = 65$ K, $\epsilon = 0.46$, $J_{\pi}/J = 0.2$, $J_{\pi/2}/J = 0.2$, and $g = 6.2$. The calculated intensities are presented with the scale given in color bar. The symbols are the experimental resonance points obtained from the previous ESR measurements [17].

$$P_j^y = (A \cos(\pi j) + D)(S_j^y S_{j+1}^z - S_j^z S_{j+1}^y) - (B - E) \cos\left(\frac{\pi}{2} j\right) (S_j^y S_{j+1}^y - S_j^x S_{j+1}^x), \quad (8)$$

$$P_j^z = (B + E) \left[\sin\left(\frac{\pi}{2} j\right) (S_j^y S_{j+1}^z - S_j^z S_{j+1}^y) - \cos\left(\frac{\pi}{2} j\right) (S_j^z S_{j+1}^x - S_j^x S_{j+1}^z) \right], \quad (9)$$

where, A , B , E , and D are constants, determined by $C_{\beta\gamma}$ with $\beta, \gamma = X, Y, Z$, and the angle between the z and Z (see Appendix C). Owing to the π and $\pi/2$ periodicities of P_j , the uniform oscillation of the electric fields can couple with magnetic excitation at $q_z = \pi$ and $\pi/2$, thereby resulting in electric dipole transitions. We examine the above two mechanisms by numerical calculations via the density matrix renormalization group (DMRG) method with parameters $J = 65$ K, $\epsilon = 0.46$, $J_{\pi}/J = 0.2$, $J_{\pi/2}/J = 0.2$, and $g = 6.2$. The dynamical DMRG ran with 128 sites and the number of states kept in the renormalization steps was 40. We calculate the dynamical structure factor given by

$$S^{\alpha}(q, \omega) = -\frac{1}{\pi} \text{Im} \langle \Psi_G | S_q^{\alpha \dagger} \frac{1}{\omega + E_G - \mathcal{H} + i\eta} S_q^{\alpha} | \Psi_G \rangle, \quad (10)$$

where S_q^{α} represents the Fourier transform of the α component of the spin, $|\Psi_G\rangle$ depicts the ground state and η is a small broadening factor set to 0.05 in the unit of J . For $S^z(q=0, \omega)$, a Lorentzian peak at zero energy is subtracted because of finite magnetic moments induced by the magnetic field. We also

calculate the transverse structure factor for the electric dipole transition given as

$$T_{\pi, \pi/2}^x(\omega) = -\frac{1}{\pi} \text{Im} \langle \Psi_G | P_{\pi, \pi/2}^{\dagger} \frac{1}{\omega + E_G - \mathcal{H} + i\eta} P_{\pi, \pi/2}^x | \Psi_G \rangle, \quad (11)$$

where $P_{\pi}^x = \sum_j \cos(\pi j) (S_j^z S_{j+1}^x - S_j^x S_{j+1}^z)$ and $P_{\pi/2}^x = \sum_j \sin(\frac{\pi}{2} j) (S_j^x S_{j+1}^y - S_j^y S_{j+1}^x)$. Figure 4 display the comparisons between the calculations and the experimental resonance points. As shown in Fig. 4(a), in $S^x(q=0, \omega)$, which gives the probability for the transitions by oscillating magnetic field along the x , weak intensity appears for the P mode in addition to the strong intensity for the spinon excitation and B mode, as observed in the experiment. The calculation suggests that in the fully spin-polarized state above H_s , the slope of P becomes twice as large as those of the one magnon excitation modes such as $Q_{L,H}$, L , and B . This indicates that P unambiguously originates from the two-string excitation, which changes to the two magnon bound state above H_s . Different from the experimental results, $S^x(q=0, \omega)$ gives no intensity for the Q_H above H_s . Because a state at $q_z = \pi$ with a flip of two neighboring spins from the fully spin-polarized state is mixed with the ground state by the $S_j^- S_{j+1}^-$ term in \mathcal{H}_{π} , one magnon excitation at $q_z = \pi$ from this mixed ground state seems to be feasible by oscillating magnetic field along the x . However, the magnetic dipole transition between one magnon and such two-spin flipped states at $q_z = \pi$ is prohibited by the parity difference between these two states. The former and the later states possess

fixed parities of odd and even, respectively. The magnetic dipole transition between such parity different states is prohibited because the S_q^x with $q = 0$ has even parity. One possible mechanism for the finite magnetic dipole transition probability for the Q_H in the experimental situation is the second nearest-neighbor exchange interaction with inclined principle axes, which may perturb the parity symmetry of the two-magnon states mixed in the ground state. In contrast, the $T_\pi^x(\omega)$, shown in Fig. 4(d), indicates the finite probability of the electric dipole transition for the Q_L . As aforementioned, we consider that the excitation to the one-magnon state at $q = (\pi \ \pi \ \pi)$ is induced by the electric dipole transition. Because the nearest-neighbor Co-O chains in $\text{BaCo}_2\text{V}_2\text{O}_8$ are transferred by the space inversion of each other, the signs of the coefficients $C_{\beta\gamma}$ are opposite between the nearest-neighbor chains. Therefore, the spin oscillations with opposite phases between the nearest-neighbor chains to each other, induced by the magnon excitation at $q = (\pi \ \pi \ \pi)$, cause a uniform oscillation of the electric polarization, resulting in the electric dipole transition, whereas the magnon at $q = (0 \ 0 \ \pi)$, which induces the spin oscillations with the same phase between the chains, is observed by the magnetic dipole transition. Next, $S^z(q = 0, \omega)$ and $T_{\pi/2}^x(\omega)$ shown in Figs. 4(b) and 4(c), respectively, indicate that as the magnetic field is increased, the L gradually changes from electric dipole active by $\mathbf{e} \perp \mathbf{c}$ to magnetic dipole active by $\mathbf{h} \parallel \mathbf{c}$ around 16 T, in agreement with the experiment. A slight deviation of the resonance points from the intensity peak of $S^z(q = 0, \omega)$ above H_s comes from the fact that the second nearest-neighbor interaction, which was included in our previous analysis [17], is neglected in the present DMRG calculations. Figure 4(c) also demonstrates that the M is electroactive, as observed in the experiment. The rather strong intensity of the two-magnon bound state is observed in $S^z(q = 0, \omega)$ for $H > H_s$, as presented in Fig. 4(b), owing to the mixing of this bound state to the fully spin-polarized ground state by \mathcal{H}_π . We also consider that the observations of the excitations at $q = \pi/2$ with large gaps at zero magnetic field by the far-infrared spectroscopy measurements in $\text{SrCo}_2\text{V}_2\text{O}_8$ [52] are also owing to the perturbative interactions from the four-fold screw structure of the Co-O chain.

The above discussions show that the DMRG calculations, considering the four- and two-fold periodical interactions and the spin-dependent electric polarization, elucidated the general results of the high-field ESR experiments. These perturbative interactions are also considered to affect the ground-state properties of $\text{BaCo}_2\text{V}_2\text{O}_8$. Figure 4(d) presents the finite intensity of the $T_\pi^x(\omega)$ at zero frequency in the field region from approximately 12 T to H_s . The Bethe ansatz calculation indicated that the staggered correlation of the transverse spin component develops more dominantly in the quantum critical ground state than the incommensurate longitudinal correlation in this field region [20]. This staggered correlation plus longitudinal magnetization along the z -axis, induced by the external magnetic field, generates the vector spin chirality $\mathbf{S}_j \times \mathbf{S}_{j+1}$, which is directed perpendicularly to z . Because this vector spin chirality change its sign alternatively along the chain reflecting the staggered correlation, the P_π^x shows positive correlation in the ground state, resulting in the finite intensity of the $T_\pi^x(\omega)$ at $\omega = 0$ seen

in Fig. 4(d). When this staggered spin correlation develops to the long-range transverse Néel order owing to the interchain interactions as suggested from the previous neutron diffraction [53], the static electric polarization perpendicular to c should appear in a chain. Hence, the transverse Néel ordered state, which appears in a higher field region than the SDW phase, is considered to be antiferroelectric state, in which the electric polarizations in the chains align oppositely between the nearest or second nearest-neighbor chains in $\text{BaCo}_2\text{V}_2\text{O}_8$. From the NMR measurements, rather complex phase diagram, in which the magnetic order is significantly suppressed around H_a , was reported [54]. We consider that this suppression is attributable to the softening of the magnetic excitation L at $q_z = \pi/2$, observed around H_a . The mixing of the magnetic excited state with $\pi/2$ periodicity to the ground state by $\mathcal{H}_{\pi/2}$ is enhanced around H_a , as indicated by the enhanced intensity in $S^z(q = 0, \omega)$ for L . This enhanced mixing probably disturbs the staggered magnetic ordering around H_a . A tiny hump in the magnetization curves around H_a in $\text{BaCo}_2\text{V}_2\text{O}_8$ [17] must also emerge from this mixing.

V. CONCLUSION

In conclusion, we clarified the optical selection rules of the magnetic excitation in $\text{BaCo}_2\text{V}_2\text{O}_8$, in longitudinal magnetic fields by measuring the polarization dependence of the ESR spectra. The spinon and the psinon-antispinon excitation, labeled as B , at $q = 0$, which are allowed for magnetic dipole transition, are induced by the transverse oscillating magnetic field. In contrast, the psinon-psinon excitation L at $q_z = \pi/2$ changes from electroactive by $\mathbf{e} \perp \mathbf{c}$ to magnetoactive by $\mathbf{h} \parallel \mathbf{c}$ around H_a . The two string excitation P at $q_z = \pi$ is magnetoactive by $\mathbf{h} \perp \mathbf{c}$, whereas the M at $q_z = \pi/2$ is electroactive by $\mathbf{e} \perp \mathbf{c}$. The one magnon excitation Q_H at $q = (0 \ 0 \ \pi)$ and Q_L at $q = (\pi \ \pi \ \pi)$ in the fully spin-polarized state are suggested to be magneto- and electroactive, respectively. These results indicate overall agreement with our calculations, considering the mixing of the quantum states by two- and four-fold periodical interactions, generated from the four-fold screw structure of the Co-O chain and the spin-dependent electric dipoles. This work has demonstrated that the screw chain structure, which generates periodic perturbative interactions, in addition to the coupling between spins and electric dipole, offers novel opportunities to explore unconventional low-lying magnetic excitation in quantum magnets with high accuracies via high-field ESR and terahertz spectroscopy measurements.

ACKNOWLEDGMENTS

The authors thank M. Kohno, M. Matsumoto, and H. Matsueda for their valuable discussions. The experimental work was performed at the High Field Laboratory for Superconducting Materials, Institute for Materials Research, Tohoku University (Project No. 19H0406) and at the Center for Advanced High Magnetic Field Science in Osaka University under the Visiting Researcher's Program of the Institute for Solid State Physics, The University of Tokyo. The computations were performed using supercomputers at the Japan Atomic Energy Agency and at the Institute for Solid State

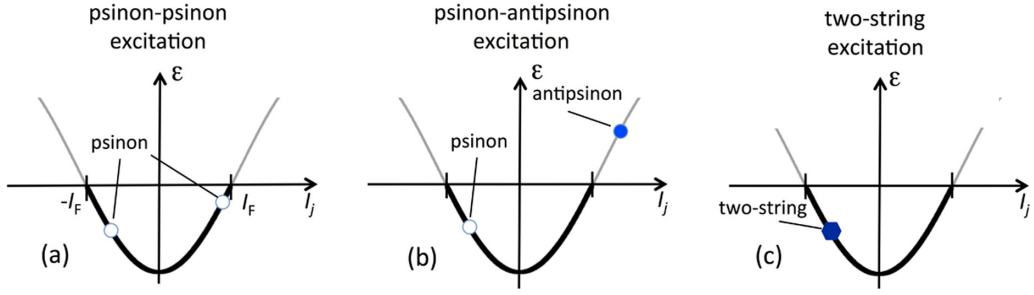


FIG. 5. Schematic pictures for distribution of the Bethe quantum numbers I_j for (a) psinon-psinon, (b) antipsinon-psinon, and (c) two-string excitation. $I_F = N/4 - M/2 - 1/2$ is the maximum Bethe quantum number, which is occupied by the magnon in the ground state. Thus, a region shown by a bold curve is occupied by the magnons in the ground state. Note that the energy dispersion ϵ is not precisely depicted and is nonlinearly renormalized by changes in the distribution of the I_j 's due to the interaction effect among spins.

Physics, The University of Tokyo. This work was, in part, supported by the Grant-in-Aid for Scientific Research (Grants No. 19H01834, No. 19K03678, No. 19K03745, No. 21H01026, and No. 21H05191) from MEXT Japan.

APPENDIX A: MAGNETIC EXCITATION OF THE $S = \frac{1}{2}$ ANTIFERROMAGNETIC QUANTUM SPIN CHAIN IN MAGNETIC FIELDS

In the Bethe ansatz calculation for the $S = \frac{1}{2}$ antiferromagnetic quantum spin chain, a state with the spins fully polarized along the magnetic field is taken as the reference state, namely the vacuum state. Then the all eigenstates are obtained by inducing magnons, which correspond to overturned spins from the fully polarized spin state, into the vacuum. The induced magnons are labeled by the Bethe quantum numbers I_j ($j = 1 \sim M$), where the M is magnetization. The I_j takes an integer or half-integer depending on the total number N of spins in the chain and M . The ground state with the magnetization M is specified by a set of the I_j 's [9,10]

$$\{I_j\}_G = \left\{ -\frac{N}{4} + \frac{M}{2} + \frac{1}{2}, \dots, \frac{N}{4} - \frac{M}{2} - \frac{1}{2} \right\}. \quad (\text{A1})$$

The distribution of I_j in the ground state is somewhat analogous to the momentum distribution of spinless fermions as shown by bold curves in Fig. 5. The lowest magnetic excitation from the ground state with finite M is obtained by pair creation of the quasiparticles psinon and/or antipsinon. The psinon (antipsinon) is hole (particle) created inside (outside) the $\{I_j\}_G$ as shown in Figs. 5(a) and 5(b) [9,10]. By substituting a set of the Bethe quantum numbers for magnons and antipsinons to the Bethe ansatz equation, a set of real rapidities $\{\Lambda_j\}$ are derived, and then the eigenenergy, wave function, and momentum of the quantum spin chain are obtained from the $\{\Lambda_j\}$. There are also the solutions with complex rapidities, which is known as the n -string state ($n \geq 2$). The n -string is given by a set of n rapidities, expressed as $\Lambda_j = \bar{\Lambda} + i(n+1-2j)$ for $j = 1 \sim n$, where $\bar{\Lambda}$ is real [8,13–15]. The Bethe quantum number, which specifies the complex rapidity for two string state is denoted by a hexagon in Fig. 5(c). Upon increasing the magnetic field, n -string state changes asymptotically to the n magnon bound state in the fully polarized spin state above the saturation field.

APPENDIX B: EFFECTIVE HAMILTONIAN FOR THE FOUR-FOLD SCREW SPIN CHAIN

We derive the effective intrachain exchange interactions for the four-fold screw spin chain in $\text{BaCo}_2\text{V}_2\text{O}_8$ by taking into account the inclination of the principal axes of the CoO_6 octahedra. The anisotropic exchange interaction between the j and $j+1$ sites on the chain, is given as

$$\mathcal{H}_j = S_j \tilde{J} S_{j+1}, \quad (\text{B1})$$

with

$$\tilde{J} = \begin{pmatrix} J_\xi & 0 & 0 \\ 0 & J_\eta & 0 \\ 0 & 0 & J_\zeta \end{pmatrix}. \quad (\text{B2})$$

The $\xi\eta\zeta$ -coordinate system is inclined from the xyz -system by an angle θ around the y -axis, and then is rotated by $\phi = (\pi/2)j$ around the z -axis, where the ξ, η, ζ and the x, y, z are the principal axes of the anisotropic exchange interaction and those of the crystal lattice with x, y and z parallel to the [100], [010], and [001], respectively. \tilde{J} in the xyz -coordinate system is expressed by a symmetric tensor

$$\begin{pmatrix} J_{xx} & J_{xy} & J_{xz} \\ J_{xy} & J_{yy} & J_{yz} \\ J_{xz} & J_{yz} & J_{zz} \end{pmatrix}, \quad (\text{B3})$$

with

$$J_{xx} = (J_\xi \cos^2\theta + J_\zeta \sin^2\theta) \cos^2\phi + J_\eta \sin^2\phi, \quad (\text{B4})$$

$$J_{yy} = (J_\xi \cos^2\theta + J_\zeta \sin^2\theta) \sin^2\phi + J_\eta \cos^2\phi, \quad (\text{B5})$$

$$J_{zz} = J_\xi \sin^2\theta + J_\zeta \cos^2\theta, \quad (\text{B6})$$

$$J_{xy} = (J_\xi \cos^2\theta - J_\eta + J_\zeta \sin^2\theta) \sin\phi \cos\phi, \quad (\text{B7})$$

$$J_{xz} = (J_\zeta - J_\xi) \sin\theta \cos\theta \cos\phi, \quad (\text{B8})$$

$$J_{yz} = (J_\zeta - J_\xi) \sin\theta \cos\theta \sin\phi. \quad (\text{B9})$$

The total Hamiltonian \mathcal{H} for the screw spin chain is obtained by taking a sum of \mathcal{H}_j through the chain. As described in the main text, the \mathcal{H} is expressed as

$$\mathcal{H} = \mathcal{H}_{\text{uni}} + \mathcal{H}_\pi + \mathcal{H}_{\pi/2}, \quad (\text{B10})$$

with

$$\mathcal{H}_{\text{uni}} = \sum_j J \left\{ S_j^z S_{j+1}^z + \frac{\epsilon}{2} (S_j^+ S_{j+1}^- + S_j^- S_{j+1}^+) \right\} - g\mu_B H S_j^z, \quad (\text{B11})$$

$$\mathcal{H}_\pi = \sum_j J_\pi \{ \cos(\pi j) (S_j^+ S_{j+1}^+ + S_j^- S_{j+1}^-) \}, \quad (\text{B12})$$

and

$$\mathcal{H}_{\pi/2} = \sum_j J_{\pi/2} \left\{ \cos\left(\frac{\pi}{2}j\right) (S_j^x S_{j+1}^z + S_j^z S_{j+1}^x) + \sin\left(\frac{\pi}{2}j\right) (S_j^y S_{j+1}^z + S_j^z S_{j+1}^y) \right\}. \quad (\text{B13})$$

Here J , J_π , $J_{\pi/2}$ and ϵ are given as

$$J = J_{zz}, \quad (\text{B14})$$

$$J_\pi = \frac{1}{4}(J_\xi \cos^2\theta - J_\eta + J_\zeta \sin^2\theta), \quad (\text{B15})$$

$$J_{\pi/2} = \frac{1}{4}(J_\zeta - J_\xi) \sin 2\theta, \quad (\text{B16})$$

$$\epsilon = J_{\text{uni}}/J_{zz}, \quad (\text{B17})$$

with

$$J_{\text{uni}} = \frac{1}{2}(J_\xi \cos^2\theta + J_\eta + J_\zeta \sin^2\theta). \quad (\text{B18})$$

APPENDIX C: SPIN-DEPENDENT ELECTRIC POLARIZATION IN THE SCREW SPIN CHAIN IN BaCo₂V₂O₈

The electric polarization \mathbf{P}_j , which depends on the vector spin chirality $\mathbf{S}_j \times \mathbf{S}_{j+1}$ between the two nearest-neighbor spins on the j - and $j+1$ -sites, is generally expressed as

$$\mathbf{P}_j = \tilde{\mathbf{C}}(\mathbf{S}_j \times \mathbf{S}_{j+1}), \quad (\text{C1})$$

where $\tilde{\mathbf{C}}$ is a second rank axial tensor [34]. The form of the $\tilde{\mathbf{C}}$ is restricted by the crystallographic symmetry between the

two spin sites [51]. In the spin chain of BaCo₂V₂O₈, the nearest-neighbor Co²⁺ sites are connected by the two fold rotation around the [100] or [010] axis [38]. In this case, $\tilde{\mathbf{C}}$ is given as

$$\tilde{\mathbf{C}} = \begin{pmatrix} 0 & C_{XY} & 0 \\ C_{YX} & 0 & C_{YZ} \\ 0 & C_{ZY} & 0 \end{pmatrix}, \quad (\text{C2})$$

where the Z parallel to the nearest neighbor Co-Co bond, Y parallel to the [010], and X perpendicular to both Y and Z . Similar to the $\tilde{\mathbf{J}}$, mentioned in the above section, the principal axes of $\tilde{\mathbf{C}}$ are inclined by an angle ψ around the y -axis, and then are rotated by $\phi = (\pi/2)j$ around the z -axis. The $\tilde{\mathbf{C}}$ is expressed in the xyz -coordinate as

$$\begin{pmatrix} -A \sin 2\phi & A \cos 2\phi + D & (B - E) \sin \phi \\ A \cos 2\phi - D & A \sin 2\phi & -(B - E) \cos \phi \\ (B + E) \sin \phi & -(B + E) \cos \phi & 0 \end{pmatrix}, \quad (\text{C3})$$

where

$$A = C_{XY}^s \cos \psi + C_{YZ}^s \sin \psi, \quad (\text{C4})$$

$$B = C_{XY}^s \sin \psi - C_{YZ}^s \cos \psi, \quad (\text{C5})$$

$$D = C_{XY}^a \cos \psi - C_{YZ}^a \sin \psi, \quad (\text{C6})$$

$$E = C_{XY}^a \sin \psi + C_{YZ}^a \cos \psi, \quad (\text{C7})$$

where $C_{\beta\gamma}^s$ and $C_{\beta\gamma}^a$ ($\beta, \gamma = X, Y, Z$) are the symmetric and asymmetric components of the $\tilde{\mathbf{C}}$, namely,

$$C_{\beta\gamma}^s = \frac{1}{2}(C_{\beta\gamma} + C_{\gamma\beta}), \quad (\text{C8})$$

$$C_{\beta\gamma}^a = \frac{1}{2}(C_{\beta\gamma} - C_{\gamma\beta}). \quad (\text{C9})$$

Therefore, the electric polarization \mathbf{P}_j is expressed in the xyz -coordinate as following:

$$P_j^x = [A \cos(\pi j) + D](\mathbf{S}_j \times \mathbf{S}_{j+1})_y + (B - E) \sin\left(\frac{\pi j}{2}\right) (\mathbf{S}_j \times \mathbf{S}_{j+1})_z, \quad (\text{C10})$$

$$P_j^y = [A \cos(\pi j) + D](\mathbf{S}_j \times \mathbf{S}_{j+1})_x - (B - E) \cos\left(\frac{\pi j}{2}\right) (\mathbf{S}_j \times \mathbf{S}_{j+1})_z, \quad (\text{C11})$$

$$P_j^z = (B + E) \left[\sin\left(\frac{\pi j}{2}\right) (\mathbf{S}_j \times \mathbf{S}_{j+1})_x - \cos\left(\frac{\pi j}{2}\right) (\mathbf{S}_j \times \mathbf{S}_{j+1})_y \right]. \quad (\text{C12})$$

- [1] H. Bethe, *Z. Phys.* **71**, 205 (1931).
 [2] J. Des Cloizeaux and J. J. Pearson, *Phys. Rev.* **128**, 2131 (1962).
 [3] T. Yamada, *Prog. Theor. Phys.* **41**, 880 (1969).
 [4] Y. Endoh, G. Shirane, R. J. Birgeneau, P. M. Richards, and S. L. Holt, *Phys. Rev. Lett.* **32**, 170 (1974).
 [5] G. Müller, H. Thomas, H. Beck, and J. C. Bonner, *Phys. Rev. B* **24**, 1429 (1981).
 [6] L. D. Faddeev and L. A. Tahhtrajan, *Phys. Lett. A* **85**, 375 (1981).
 [7] M. Karbach, K. Hu, and G. Müller, *Comp. Phys.* **12**, 565 (1998).

- [8] C. N. Yang and C. P. Yang, *Phys. Rev.* **151**, 258 (1966).
 [9] M. Karbach and G. Müller, *Phys. Rev. B* **62**, 14871 (2000).
 [10] M. Karbach, D. Biegel, and G. Müller, *Phys. Rev. B* **66**, 054405 (2002).
 [11] N. Ishimura and H. Shiba, *Prog. Theor. Phys.* **57**, 1862 (1977).
 [12] D. C. Dender, P. R. Hammar, D. H. Reich, C. Broholm, and G. Aeppli, *Phys. Rev. Lett.* **79**, 1750 (1997).
 [13] M. Takahashi, *Prog. Theor. Phys.* **46**, 401 (1971).
 [14] M. Gaudin, *Phys. Rev. Lett.* **26**, 1301 (1971).
 [15] M. Kohno, *Phys. Rev. Lett.* **102**, 037203 (2009).
 [16] W. Yang, J. Wu, S. Xu, Z. Wang, and C. Wu, *Phys. Rev. B* **100**, 184406 (2019).

- [17] S. Kimura, H. Yashiro, K. Okunishi, M. Hagiwara, Z. He, K. Kindo, T. Taniyama, and M. Itoh, *Phys. Rev. Lett.* **99**, 087602 (2007).
- [18] F. D. M. Haldane, *Phys. Rev. Lett.* **45**, 1358 (1980).
- [19] K. Okunishi and T. Suzuki, *Phys. Rev. B* **76**, 224411 (2007).
- [20] S. Kimura, T. Takeuchi, K. Okunishi, M. Hagiwara, Z. He, K. Kindo, T. Taniyama, and M. Itoh, *Phys. Rev. Lett.* **100**, 057202 (2008).
- [21] S. Kimura, M. Matsuda, T. Masuda, S. Hondo, K. Kaneko, N. Metoki, M. Hagiwara, T. Takeuchi, K. Okunishi, Z. He, K. Kindo, T. Taniyama, and M. Itoh, *Phys. Rev. Lett.* **101**, 207201 (2008).
- [22] E. Canévet, B. Grenier, M. Klanjšek, C. Berthier, M. Horvatić, V. Simonet, and P. Lejay, *Phys. Rev. B* **87**, 054408 (2013).
- [23] Q. Faure, S. Takayoshi, V. Simonet, B. Grenier, M. Månsson, J. S. White, G. S. Tucker, C. Rüegg, P. Lejay, T. Giamarchi, and S. Petit, *Phys. Rev. Lett.* **123**, 027204 (2019).
- [24] Z. Wang, J. Wu, W. Yang, A. K. Bera, D. Kamenskyi, A. T. M. N. Islam, S. Xu, J. M. Law, B. Lake, C. Wu, and A. Loidl, *Nature (London)* **554**, 219 (2018).
- [25] Z. Wang, M. Schmidt, A. Loidl, J. Wu, H. Zou, W. Yang, C. Dong, Y. Kohama, K. Kindo, D. I. Gorbunov, S. Niesen, O. Breunig, J. Engelmayr, and T. Lorenz, *Phys. Rev. Lett.* **123**, 067202 (2019).
- [26] A. P. Bera, J. Wu, W. Yang, R. Bewley, M. Boehm, J. Xu, M. Bartkowiak, O. Prokhnenko, B. Klemke, A. P. Bera, A. T. M. Nazmul Islam, J. M. Law, Z. Wang, and B. Lake, *Nat. Phys.* **16**, 625 (2020).
- [27] Z. He, T. Taniyama, T. Kyômen, and M. Itoh, *Phys. Rev. B* **72**, 172403 (2005).
- [28] Z. He, D. Fu, T. Taniyama, T. Kyômen, and M. Itoh, *Chem. Mater.* **17**, 2924 (2005).
- [29] P. Lejay, E. Canévet, S. K. Srivastava, B. Grenier, M. Klanjšek, and C. Berthier, *J. Cryst. Growth* **317**, 128 (2011).
- [30] H. Shiba, *Prog. Theor. Phys.* **64**, 466 (1980).
- [31] B. Grenier, S. Petit, V. Simonet, E. Canévet, L.-P. Regnault, S. Raymond, B. Canals, C. Berthier, and P. Lejay, *Phys. Rev. Lett.* **114**, 017201 (2015).
- [32] Z. Wang, M. Schmidt, A. K. Bera, A. T. M. N. Islam, B. Lake, A. Loidl, and J. Deisenhofer, *Phys. Rev. B* **91**, 140404(R) (2015).
- [33] T. Sakai and H. Shiba, *J. Phys. Soc. Jpn.* **63**, 867 (1994).
- [34] T. Moriya, *J. Phys. Soc. Jpn.* **21**, 926 (1966).
- [35] Y. Tokura, S. Seki, and N. Nagaosa, *Rep. Prog. Phys.* **77**, 076501 (2014).
- [36] M. Akaki, D. Yoshizawa, A. Okutani, T. Kida, J. Romhányi, K. Penc, and M. Hagiwara, *Phys. Rev. B* **96**, 214406 (2017).
- [37] S. Kimura, M. Matsumoto, M. Akaki, M. Hagiwara, K. Kindo, and H. Tanaka, *Phys. Rev. B* **97**, 140406(R) (2018).
- [38] R. Wichmann and H. Müller-Buschbaum, *Z. Anorg. Allg. Chem.* **534**, 153 (1986).
- [39] Q. Faure, S. Takayoshi, S. Petit, V. Simonet, S. Raymond, L.-P. Regnault, M. Boehm, J. S. White, M. Månsson, C. Rüegg, P. Lejay, B. Canals, T. Lorenz, S. C. Furuya, T. Giamarchi, and B. Grenier, *Nat. Phys.* **14**, 716 (2018).
- [40] Y. Cui, H. Zou, N. Xi, Zhangzhen He, Y. X. Yang, L. Shu, G. H. Zhang, Z. Hu, T. Chen, Rong Yu, J. Wu, and Yu. Weiqiang, *Phys. Rev. Lett.* **123**, 067203 (2019).
- [41] Z. Zhang, K. Amelin, X. Wang, H. Zou, J. Yang, U. Nagel, T. Rößm, T. Dey, A. A. Nugroho, T. Lorentz, J. Wu, and Z. Wang, *Phys. Rev. B* **101**, 220411(R) (2020).
- [42] A. Okutani, H. Onishi, S. Kimura, T. Takeuchi, T. Kida, M. Mori, A. Miyake, M. Tokunaga, K. Kindo, and M. Hagiwara, *J. Phys. Soc. Jpn.* **90**, 044704 (2021).
- [43] H. Zou, Y. Cui, X. Wang, Z. Zhang, J. Yang, G. Xu, A. Okutani, M. Hagiwara, M. Matsuda, G. Wang, G. Mussardo, K. Hódsági, M. Kormos, Z. Z. He, S. Kimura, R. Yu, W. Yu, J. Ma, and J. Wu, *Phys. Rev. Lett.* **127**, 077201 (2021).
- [44] S. Kimura, K. Okunishi, M. Hagiwara, K. Kindo, Z. He, T. Taniyama, M. Itoh, K. Koyama, and K. Watanabe, *J. Phys. Soc. Jpn.* **82**, 033706 (2013).
- [45] S. K. Niesen, G. Kolland, M. Seher, O. Breunig, M. Valldor, M. Braden, B. Grenier, and T. Lorenz, *Phys. Rev. B* **87**, 224413 (2013).
- [46] M. Matsuda, H. Onishi, A. Okutani, J. Ma, H. Agrawal, T. Hong, D. M. Pajerowski, J. R. D. Copley, K. Okunishi, M. Mori, S. Kimura, and M. Hagiwara, *Phys. Rev. B* **96**, 024439 (2017).
- [47] T. Moriya, *J. Appl. Phys.* **39**, 1042 (1968).
- [48] H. Katsura, N. Nagaosa, and A. V. Balatsky, *Phys. Rev. Lett.* **95**, 057205 (2005).
- [49] M. Mostovoy, *Phys. Rev. Lett.* **96**, 067601 (2006).
- [50] I. A. Sergienko and E. Dagotto, *Phys. Rev. B* **73**, 094434 (2006).
- [51] T. A. Kaplan and S. D. Mahanti, *Phys. Rev. B* **83**, 174432 (2011).
- [52] Z. Wang, J. Wu, S. Xu, W. Yang, C. Wu, A. K. Bera, A. T. M. Nazmul Islam, B. Lake, D. Kamenskyi, P. Gogoi, H. Engelkamp, N. Wang, J. Deisenhofer, and A. Loidl, *Phys. Rev. B* **94**, 125130 (2016).
- [53] B. Grenier, V. Simonet, B. Canals, P. Lejay, M. Klanjšek, M. Holvatić, and C. Berthier, *Phys. Rev. B* **92**, 134416 (2015).
- [54] M. Klanjšek, M. Horvatić, S. Krämer, S. Mukhopadhyay, H. Mayaffre, C. Berthier, E. Canévet, B. Grenier, P. Lejay, and E. Orignac, *Phys. Rev. B* **92**, 060408(R) (2015).